

Quantum Oscillations in a Two-Dimensional Electron Gas at the Rocksalt/Zincblende Interface of PbTe/CdTe (111) Heterostructures

Bingpo Zhang,[†] Ping Lu,[‡] Henan Liu,[§] Lin Jiao,[†] Zhenyu Ye,[†] M. Jaime,^{||} F.F. Balakirev,^{||} Huiqiu Yuan,[†] Huizhen Wu,^{*,†} Wei Pan,^{*,‡} and Yong Zhang^{*,§}

[†]Department of Physics, State Key Laboratory for Silicon Materials, and Center for Correlated Matter, Zhejiang University, Hangzhou, Zhejiang, 310027, People's Republic of China

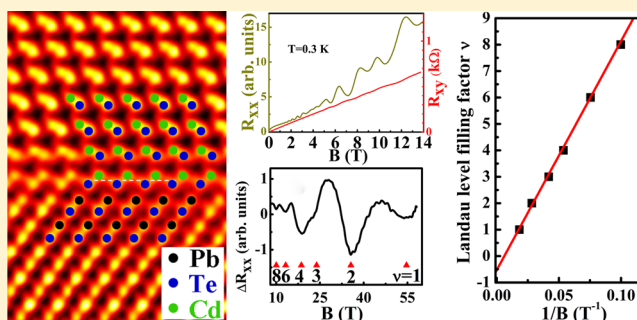
[‡]Sandia National Laboratories, Albuquerque, New Mexico 87185, United States

[§]Department of Electrical Engineering, Optoelectronics Center, University of North Carolina at Charlotte, Charlotte, North Carolina 28223, United States

^{||}NHMF, Los Alamos National Lab, Los Alamos, New Mexico 87545, United States

ABSTRACT: Quantum oscillations are observed in the 2DEG system at the interface of novel heterostructures, PbTe/CdTe (111), with nearly identical lattice parameters ($a_{\text{PbTe}} = 0.6462$ nm, $a_{\text{CdTe}} = 0.648$ nm) but very different lattice structures (PbTe: rock salt, CdTe: zinc blende). The 2DEG formation mechanism, a mismatch in the bonding configurations of the valence electrons at the interface, is uniquely different from the other known 2DEG systems. The aberration-corrected scanning transmission electron microscope (AC-STEM) characterization indicates an abrupt interface without cation interdiffusion due to a large miscibility gap between the two constituent materials. Electronic transport measurements under magnetic field up to 60 T, with the observation of Landau level filling factor $\nu = 1$, unambiguously reveal a π Berry phase, suggesting the Dirac Fermion nature of the 2DEG at the heterostructure interface, and the PbTe/CdTe heterostructure being a new candidate for 2D topological crystalline insulators.

KEYWORDS: PbTe/CdTe (111), 2DEG, quantum oscillations, Berry phase, topological insulator



The two-dimensional electron gas (2DEG) at the interface of two materials with same crystal symmetry and similar lattice constants but different bandgaps has for many years been a fertile playground for discovering novel electron physics and new device applications. History has shown ample examples of novel physics associated with heterojunction interfaces, for example, the fractional quantum Hall effect in the 2DEG in GaAs/AlGaAs heterostructures,¹ high-brightness InGaN/AlGaN blue light-emitting diodes,² superconductivity at the LaAlO₃/SrTiO₃ interface,³ and the quantum spin Hall effect in HgTe/CdTe heterojunctions.⁴ This work reports the first observation of quantum oscillations in a 2DEG realized at the interface of an unusual heterostructure, PbTe (rock-salt)/CdTe (zinc-blende),⁵ where the primary mechanism is the mismatch in the bonding coordination at the interface, distinctly different from the other 2DEG systems. This work also suggests that the 2DEG at the interface may be a Dirac electron system with a nonzero Berry phase,⁶ indicating the topological nature of the 2DEG in this novel heterostructure. PbTe is a well-known and widely used semiconductor. Indeed, with unique properties such as a narrow, direct band gap of ~ 0.3 eV, high electron mobility, and a large dielectric constant, PbTe is of great interest in applications including thermal-electrics,⁷ mid-

infrared (MIR) emitter,⁸ sensor,⁹ etc. Recently, this material system and in particular Pb_{1-x}Sn_xTe alloy and SnTe systems have received a great deal of interest, due to the theoretical prediction that Pb_{1-x}Sn_xTe and SnTe may be a topological crystalline insulator (TCI),¹⁰ where the insulating bulk is accompanied by helical Dirac-like surface states. In contrast with conventional topological insulators,¹¹⁻¹³ where the surface states are protected by time-reversal symmetry, in TCI the topological nature of electron structures arises from the crystalline symmetries.¹⁴ Consequently, the surface states are more robust against disorder. Subsequent experiments seem to confirm that indeed SnTe¹⁵ and Pb_{1-x}Sn_xTe^{16,17} are topological crystalline insulators. More recently, it has been predicted that TCI may exist in 2D-TCIs of SnTe and Pb_{1-x}Sn_xTe thin films.¹⁸ Up to date, studies on TCIs are all carried out either in bulk crystals or thin films, and no research activity has been explored in heterostructures.

Recently, a structure-mismatched CdTe/PbTe heterostructure, in which PbTe crystallizes in a rock-salt (RS) structure

Received: February 9, 2015

Revised: May 23, 2015

Published: June 5, 2015



and CdTe in a zinc-blende (ZB) structure, has attracted much attention due to its promise for fabrication of MIR optoelectronic and spintronic devices.^{8,19,20} For instance, PbTe quantum dots (QDs) embedded in CdTe matrices were found to exhibit intense MIR luminescence above room temperature;¹⁹ abnormal enhancement of MIR light emission was also observed from the CdTe/PbTe (111) heterostructure, attributed to the inherent (111) polar interface and coupling of surface plasmon localized at the metallic CdTe/PbTe interface to light emitted from the narrow gap PbTe.²¹ This work is inspired by the recent experimental finding of high concentration and high mobility electrons derived from conventional Hall measurements in PbTe/CdTe (111) heterostructures, and the theoretical prediction of the formation of 2DEG at the interface.⁵

In this Letter, we present results on electronic transport properties of the 2DEG realized at the interfaces of PbTe/CdTe (111) heterostructures as well as high-resolution TEM probe of the atomic structure of the interface and other material characterizations. Compared to the other better known heterostructures, the (111) interface between PbTe and CdTe is unique. It is known that PbTe grows in the RS structure while CdTe grows as ZB. As a consequence, the (111) interface between PbTe and CdTe⁵ is dramatically different from all known interfaces where 2DEGs are realized. The mismatch in crystal structure between PbTe and CdTe leads to a mismatch in the bonding configurations of the valence electrons. In this regard, a systematical study of the 2DEG in this peculiar heterostructure is guaranteed for potentially exotic electron physics in this new system. Indeed, evidence of topological surface states is observed in this material system in low-temperature electronic transport measurements.

The microscopic scale information on the interfacial structure is pivotal for understanding the underlying mechanism of the 2DEG formation. Figure 1 shows the arrangement of atoms near the PbTe/CdTe interface obtained from an aberration-corrected scanning transmission electron microscope (AC-STEM) taken with a high-angle annular dark-field

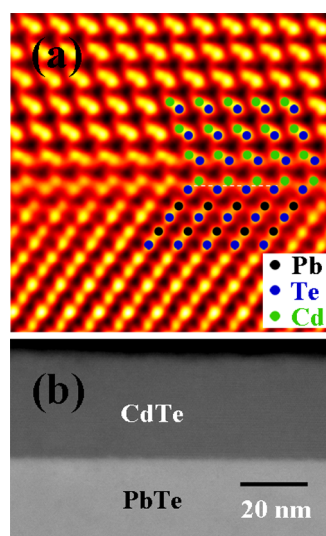


Figure 1. (a) Aberration-corrected scanning transmission electron microscope (AC-STEM) image of a PbTe/CdTe heterostructure, showing the arrangement of atoms near the interface. (b) Low-magnification TEM image of the PbTe/CdTe heterostructure.

(HAADF) detector. The STEM-HAADF imaging allows for direct column-by-column mapping of the interfacial structure. The high-resolution image Figure 1a reveals atomic level details of the interface, in particular, a highly distorted first CdTe monolayer. Figure 1b shows a low-magnification image of the heterostructure. Clearly, the interfacial Te layer is shared by PbTe and CdTe, which leads to an unusual bonding configurations for the Te atoms of the interfacial layer. On the PbTe side, each Te atom is coordinated with three Pb atoms (because of the 6-fold coordination of RS), whereas on the CdTe side, it is coordinated with three Cd atoms (because of the 4-fold coordination of ZB). In the simplest consideration based on electron counting, i.e., assuming full ionicity and no charge redistribution, on average, the Te atom should receive 1.0 electron (6p) from the three Pb atoms and 1.5 electron (5s) from the three Cd atoms, implying an excess of valence electrons with total 8.5 valence electrons, thus yielding a metallic interfacial layer. This picture is qualitatively consistent with density-functional theory (DFT) modeling.⁵ A rough estimate using the atomic density of the ZB (111) plane gives an upper value of the 2DEG as $0.5 \times (8/\sqrt{3}a_{\text{ZB}}^2) = 5.5 \times 10^{14} \text{ cm}^{-2}$, where $a_{\text{ZB}} = 0.648 \text{ nm}$ is the lattice constant of CdTe, which is higher than the DFT value of $6.0 \times 10^{13} \text{ cm}^{-2}$. Of course, partial ionicity will reduce the electron density, and both the structural distortion of the atomic layers adjacent to the interface and the nature of the (111) polar surface will add to the complexity of the charge distribution near the interface, for instance, through a strain induced piezoelectric effect and band structure modification. The unintended background doping in both layers (typically $\sim 5 \times 10^{17} \text{ cm}^{-3}$ p-type in PbTe and $\sim 5 \times 10^{15} \text{ cm}^{-3}$ n-type in CdTe) also affects the net electron density. With this understanding, we emphasize that the primary formation mechanism of the 2DEG in the current system is distinctly different from the other known systems: GaAs/AlGaAs,¹ ZnCdSe/ZnSe,²² and SiGe/Si,²³ all due to modulation doping; GaN/AlGaN due to spontaneous polarization and the piezoelectric effect.²⁴ We further note that the PbTe/CdTe system forms an abrupt interface as revealed by the AC-STEM image, which is in stark contrast to the most known semiconductor heterostructures, such as GaAs/AlAs, that typically exhibit a strong atomic interdiffusion within the first few monolayers.²⁵ Here the interdiffusion is largely suppressed due to the mismatch in bonding configuration or crystal structure, which also manifests as a large miscibility gap between PbTe and CdTe.²⁶

In the following, we focus on the electronic transport results of the 2DEG at the interface of PbTe/CdTe heterostructures. Multiple samples with different CdTe layer thicknesses have been measured. We have found that quantum oscillations are clearly observed in samples with an intermediate thickness of CdTe, because of the currently adopted relatively simple device structure. On one hand, a thin CdTe layer might not be sufficient for confining the 2DEG to the interface; therefore, the scattering of the CdTe surface states could be a serious problem. On the other hand, since the contacts were deposited on the sample surface, a thicker CdTe layer would introduce a larger series resistance due to the semi-insulating nature of bulk crystal. Significant future improvement is possible either by adding a cap layer (e.g., ZnCdTe) to a thin CdTe layer or placing the electrodes closer to the interface for a thick CdTe layer (e.g., etching away part of CdTe). In this work, only the results from a sample with intermediate CdTe thickness are highlighted in this report: sample A with 140 nm CdTe with

magnetic field B up to 15 T. The results from sample B with 200 nm CdTe are briefly mentioned. Two additional samples, sample C and D, were also used for testing, respectively, the effect of field orientation and ultrahigh magnetic field (B up to 60 T). Detailed sample information is given in Table 1. We

Table 1. Sample Information: T_{sub} Is the Calibrated Substrate Temperature during Growth, t Is the Film Thicknesses, n_s Is the Sheet Density of 2DEG from SdH Oscillations, and ν_{int} Is the Intercept of ν vs $1/B$ Plot at $1/B = 0$

sample	PbTe layer		CdTe layer		n_s (cm^{-2})	ν_{int}
	T_{sub}	t (nm)	T_{sub}	t (nm)		
A	310	600	280	140	1.10×10^{12}	-0.34
B	310	600	280	200	1.16×10^{12}	-0.36
C	310	600	250	140		
D	310	600	250	200	2×10^{12}	-0.52

have also thermally recycled the specimens a few times. Results from each cool-down are consistent. Also, it is significant to mention that this material system is chemically stable in air after growth. Quantum oscillations were observed on samples at least 6 months after the growth, although a systematic study has not yet been performed on the aging effects.

Figure 2 shows the low temperature magnetoresistance (MR) R_{xx} and Hall resistance R_{xy} curves in sample A. The

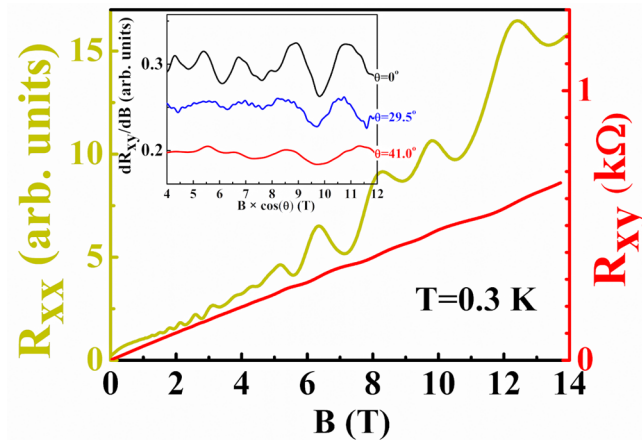


Figure 2. Magneto-resistance R_{xx} and Hall resistance R_{xy} in sample A. Quantum oscillations are observed at high magnetic fields. Plateau-like features are observed in R_{xy} at high B fields, where R_{xx} displays a strong minimum. Inset: dR_{xy}/dB versus $B \cos(\theta)$ at three selected tilting angles of the magnetic field.

measurement temperature was $T = 0.3$ K. Around zero magnetic field (B), a positive MR is observed. We believe that this positive MR is due to a multicarriers transport.²⁷ At higher fields, Shubnikov de Hass (SdH) oscillations are clearly seen on a rising, roughly linear, background. The Hall resistance displays visible plateau structures at the fields where R_{xx} shows a minimum.

In Figure 3a, we show the ΔR_{xx} after subtracting a linear background to reveal the quantum oscillations. Using the criterion of $\mu_q B = 1$ for the onset of quantum oscillations (~ 1.6 T), we can deduce the quantum mobility of $\mu_q \sim 6000 \text{ cm}^2/(\text{V s})$. We have assigned a Landau level filling factor ν to each R_{xx} minimum. In the high field regime of $B > 7$ T, ν increases by 1

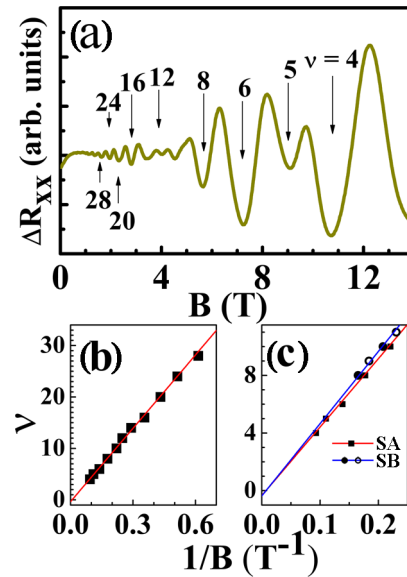


Figure 3. (a) ΔR_{xx} (obtained after subtracting a smooth background from R_{xx}) as a function of magnetic field. The arrows mark the Landau level fillings. ν increases by 1 above 7 T, where the spin degeneracy is lifted. Between 3 and 7 T, ν increases by 2. In this field range, each Landau level is spin degenerated. Below 3 T, ν increases by 4. (b) Landau level Fan diagram. The line is a linear fit to the data points. The intercept at $1/B = 0$ is -0.34 , close to -0.5 . (c) The zoomed region close to $1/B = 0$ for sample A (SA). Data from sample B (SB) are also included. The solid black circles are obtained from the R_{xx} local minima while the unfilled ones are from the local maxima in SB. In both samples, the intercept at $1/B = 0$ is close to -0.5 .

between the adjacent oscillations. In the B -field range between 3 and 7 T, ν increases by 2, due to spin degeneracy. Below 3 T, ν increases by 4, signaling the existence of an additional 2-fold degeneracy. We speculate that this 2-fold degeneracy is associated with the valley degeneracy of the PbTe [111] valleys. In Figure 3b, ν is plotted versus $1/B$. From the slope of the linear fitting, an electron density of $n_s \sim 1.1 \times 10^{12} \text{ cm}^{-2}$ is obtained. The linear extrapolation to $1/B = 0$ shows a finite y -axis intercept of -0.34 .

We notice that the density n obtained from the quantum oscillations is much smaller than that from the Hall resistance in the low magnetic field regime. There, a density of $n_H = 1.2 \times 10^{13} \text{ cm}^{-2}$ is obtained. This discrepancy indicates the coexistence of a two-dimensional electron system at the interface of PbTe/CdTe and three-dimensional bulk carriers, most likely in CdTe. This two-carrier model is also consistent with the positive MR around $B = 0$ T.²⁷ Finally, the Hall resistance R_{xy} deviates from the linear field dependence at ~ 1 T, as the 3D quantum limit is approached.²⁸ To further confirm that the quantum oscillations are of two-dimensional nature, we have also carried out tilted magnetic field studies in a different sample (sample C) grown under the same conditions. In the inset of Figure 2, we show dR_{xy}/dB versus $B \cos(\theta)$ at a few selected tilt angles. It is clearly observed that the positions of the quantum oscillation minima depends on the component of the magnetic field normal to the sample surface, thus confirming that the observed quantum oscillations are indeed due to the 2DEG at the interface of PbTe and CdTe.

Temperature dependence of SdH oscillations was carried out to deduce the effective mass of the 2DEG in our PbTe/CdTe heterostructure. In Figure 4a we show ΔR_{xx} at four temper-

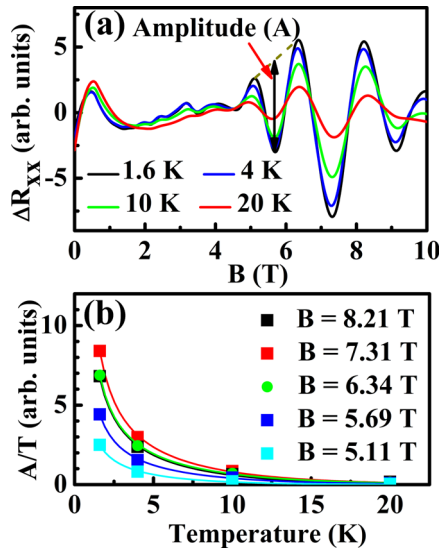


Figure 4. (a) Temperature dependence of SdH oscillations. The amplitude of oscillations is defined. (b) The amplitude of SdH oscillations versus temperature. Lines are fitted to the data points based on the formula $A/T = A_0/\sinh(2\pi^2 k_B T/\hbar\omega_c)$, as discussed in the text. The fitting at various fields all yields an effective mass of $m^* \sim 0.09m_e$.

atures of 1.6, 4, 10, and 20 K. It is clearly seen that the strongest minimum at $B \sim 7.31$ T shows virtually no shift in the B -field position at all the temperatures. This shows that the electron density is constant, at least in the temperature range below 20 K. In Figure 4b, we plot the amplitudes of the SdH oscillations, as defined as A in Figure 4a, as a function of temperature. The solid lines are the fitting curves to the data points at five different magnetic fields according to the formula $A/T = A_0/\sinh(2\pi^2 k_B T/\hbar\omega_c)$. Here A_0 is the amplitude at zero temperature and a fitting parameter, T temperature, K_B Boltzmann constant, and $\hbar\omega_c$ cyclotron energy. An effective mass of $m^* \sim 0.09 m_e$ is obtained from the fitting at all magnetic fields. The electron effective mass of the Γ valley in CdTe is $m_\Gamma \sim 0.11 m_e$,²¹ whereas the in-plane effective mass of the L valley in PbTe is rather small, $m_{\text{in-plane}} \sim 0.024m_e$.²⁹ The derived effective mass seems to suggest that the 2DEG extends into both materials.

Regarding the finite intercept at $1/B = 0$, first, we point out that a similar finite intercept was also observed in another sample (Sample B with 200 nm CdTe), as shown in Figure 3c. Second, the value of -0.34 is close to the value of -0.5 , suggesting a π Berry phase in the 2DEG at the interface of PbTe/CdTe being a Dirac-like electron system. Unlike other Berry phase systems such as 2-D graphene and bulk Rashba semiconductor BiTeI,^{30,31} our observation represents the first evidence of a nonzero Berry phase at the polar interface that consists of conventional semiconductor PbTe and CdTe. This is striking. It has been shown experimentally that, unlike $\text{Pb}_{1-x}\text{Sn}_x\text{Te}$ and SnTe, PbTe is a normal insulator. Therefore, it is surprising to observe a finite intercept in the Landau level fan diagram. On the other hand, it is known that due to the novel interface in this kind of heterostructures, the interplanar spacing of PbTe (111) in the interface region becomes alternatively wider and narrower, instead of an equal spacing of 1.87 Å in bulk PbTe.⁵ Due to the modulation in the layer spacing, in particular an increased spacing between the last PbTe monolayers, which is found to be $\sim 16\%$ from the TEM

image, a band inversion could occur in the PbTe layer in the interface region and drives the PbTe into a 2-D topological crystalline insulator.¹⁴ This induced TCI can give rise to a Berry phase in the quantum oscillations in the surface states. Moreover, the (111) orientations in PbTe and CdTe are polar. Consequently, a strong polar field can exist at the interface. This polar field, combined with strong spin-orbit coupling in PbTe and CdTe, may turn the 2DEG into a Dirac Fermion system. Indeed, this polar field induced Dirac system has been predicted in highly strained InN quantum wells.³² Of course, more measurements are needed to firmly confirm this Dirac electron system in our PbTe/CdTe heterostructures. For example, one needs to carry on magnetoresistance measurements at much higher magnetic fields so that the quantum oscillations close to Landau level filling 1 are resolved. This will make the determination of the intercept much more accurate.³³ To this purpose, we have carried out electron transport measurements up to 60 T in sample D (nominally the same as sample A) at the Pulsed Field Facility of the National High Magnetic Field Laboratory at Los Alamos National Lab. In Figure 5a and b, respectively, we show the raw R_{xx} data and

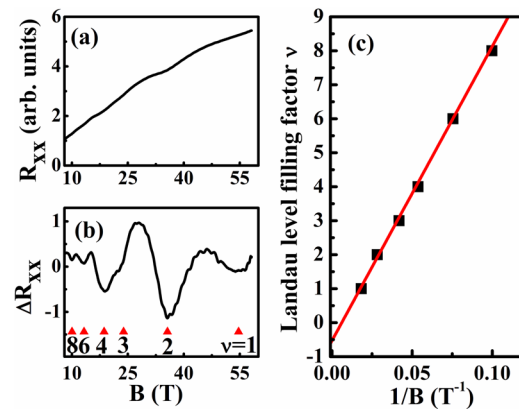


Figure 5. Sample D measured at the Pulsed Field Facility of the NHMFL at Los Alamos National Lab. (a) R_{xx} measured at ~ 1.5 K. Quantum oscillations are clearly seen. (b) R_{xx} after a smooth background is subtracted from R_{xx} in panel a. The triangles mark the positions of the Landau level filling factors $\nu = 1, 2, 4, 6,$ and 8 . (c) Landau level fan diagram. The red line is the linear fit. The intercept at $1/B = 0$ is -0.52 ± 0.07 .

ΔR_{xx} after a smooth background is subtracted. The measurement temperature was ~ 1.5 K. Quantum oscillations up to the Landau level filling $\nu = 1$ were observed. In Figure 5c, we plot ν versus $1/B$ for this sample. From the slope of the linear fit, an electron density of $n_s \sim 2 \times 10^{12} \text{ cm}^{-2}$ is obtained. The linear extrapolation to $1/B = 0$ shows a finite intercept of -0.52 ± 0.07 , more clearly indicating a Dirac system for the 2DEG in our PbTe/CdTe heterostructures.

In summary, we performed high-resolution TEM characterization of the interfacial atomic coordination of the novel PbTe/CdTe (111) heterostructure and studied the electronic transport properties of the 2DEG at the polar interface. The mismatch in the bonding configuration at the interface offers a distinctly different mechanism of 2DEG formation from the known 2DEG systems. Quantum oscillations are observed both in the magneto-resistance R_{xx} and Hall resistance R_{xy} . Evidence of a possible π Berry phase was observed by analyzing the quantum oscillations, indicating the Dirac nature of the 2D electron system at the interface. Our results suggest PbTe/

CdTe heterostructures being new candidates for topological crystalline insulators.

Methods. The PbTe/CdTe heterostructures were grown using molecular beam epitaxy technique. First, a 600 nm PbTe film was grown on a freshly cleaved BaF₂(111) substrate. Then a CdTe film of different thickness, varying from 30 to 350 nm, was epitaxially deposited on the PbTe film. The details of the growth can be found in earlier work.^{21,34} After cooling down to room temperature, the as-grown films were taken out and cut into 6 mm × 6 mm blocks and transferred immediately to an evaporator to make ohmic contacts on the four corners. First, a thin layer of 20 nm copper (>99.99%) was thermally evaporated. Afterward, a 50 nm layer of gold (>99.99%) was deposited. Both thermal depositions were done at a pressure (*P*) less than 5×10^{-3} Pa at room temperature. After contact metal depositions, the sample was annealed at 150 °C for 5 min at *P* < 0.1 Pa. Silver conductive paste was used for gold wiring.

Aberration-corrected scanning transmission electron microscope (AC-STEM) (a FEI Titan G2 80-200 STEM) was used for study of atomic-scale PbTe/CdTe (111) heterostructures. The AC-STEM image was taken with a high-angle annular dark-field (HAADF) detector which offers the atomic number sensitive imaging, so-called *Z*-contrast imaging, at a spatial resolution of better than 0.08 nm. The PbTe/CdTe interface was observed in $\langle 110 \rangle$ CdTe direction. Measurements of the transport properties were performed in a ³He cryostat with a 15 T superconducting magnet. Using a Van der Pauw configuration, four gold wires were pasted on the four Au/Cu film electrodes deposited on the CdTe surface by silver paint. The magnetic field dependence of the longitudinal resistivity *R*_{xx} and the transverse resistivity *R*_{xy} at various temperatures were measured simultaneously using a LakeShore 370 AC resistance bridge or a Stanford Research Systems SR830 lock-in amplifier.

AUTHOR INFORMATION

Corresponding Authors

*E-mail: wpan@sandia.gov.

*E-mail: yong.zhang@uncc.edu.

*E-mail: hzwwu@zju.edu.cn.

Author Contributions

H.W., W.P., and Y.Z. conceived the experiments. B.Z. carried out the material growth and device fabrication. B.Z., W.P., L.J., M.J., and F.F.B. performed the transport measurements. P.L. performed AC-STEM measurement. H.L. and H. Y. contributed to material characterizations. Z. Y. contributed to material growth. B.Z., W.P., and Y.Z. did the most writing. All authors discussed the results and commented on the manuscript.

Notes

The authors declare no competing financial interest.

ACKNOWLEDGMENTS

The work at Zhejiang University was supported by National Key Basic Research Program of China and Natural Science Foundation of China. The work at UNC-Charlotte was supported by Bissell Distinguished Professorship. The work at Sandia was supported by the Department of Energy, the Office of Basic Energy Science, Division of Material Science and Technology. Sandia National Laboratories is a multiprogram laboratory managed and operated by Sandia Corporation, a wholly owned subsidiary of Lockheed Martin Corporation, for the U.S. Department of Energy's National Nuclear Security

Administration under contract DE-AC04-94AL85000. The work at NHMFL-LANL was performed under the auspices of the National Science Foundation, Department of Energy and State of Florida. We thank Ross McDonald and Jon Bettes for helpful discussions.

REFERENCES

- (1) Tsui, D. C.; Stormer, H. L.; Gossard, A. C. *Phys. Rev. Lett.* **1982**, *48*, 1559–1562.
- (2) Nakamura, S.; Mukai, T.; Senoh, M. *Appl. Phys. Lett.* **1994**, *64*, 1687–1689.
- (3) Reyren, N.; Thiel, S.; Caviglia, A. D.; Kourkoutsis, L. F.; Hammerl, G.; Richter, C.; Schneider, C. W.; Kopp, T.; Rüetschi, A.-S.; Jaccard, D.; Gabay, M.; Müller, D. A.; Triscone, J.-M.; Mannhart, J. *Science* **2007**, *317*, 1196–1199.
- (4) König, M.; Wiedmann, S.; Brüne, C.; Roth, A.; Buhmann, H.; Molenkamp, L. W.; Qi, X. L.; Zhang, S. C. *Science* **2007**, *318*, 766–770.
- (5) Jin, S. Q.; Cai, C. F.; Bi, G.; Zhang, B. P.; Wu, H. Z.; Zhang, Y. *Phys. Rev. B* **2013**, *87*, 235315.
- (6) Novoselov, K. S.; Geim, A. K.; Morozov, S. V.; Jiang, D.; Zhang, Y.; Dubonos, S. V.; Grigorieva, I. V.; Firsov, A. A. *Science* **2004**, *306*, 666–669.
- (7) Delaire, O.; Ma, J.; Marty, K.; May, A. F.; McGuire, M. A.; Du, M.-H.; Singh, D. J.; Podlesnyak, A.; Ehlers, G.; Lumsden, M. D.; Sales, B. C. *Nat. Mater.* **2011**, *10*, 614–619.
- (8) Hochreiner, A.; Schwarzl, T.; Eibelhuber, M.; Heiss, W.; Springholz, G.; Kolkovsky, V.; Karczewski, G.; Wojtowicz, T. *Appl. Phys. Lett.* **2011**, *98*, 021106.
- (9) Maissen, C.; Masek, J.; Zogg, H.; Blunier, S. *Appl. Phys. Lett.* **1988**, *53*, 1608–1610.
- (10) Fu, L. A. *Phys. Rev. Lett.* **2011**, *106*, 106802.
- (11) Hasan, M. Z.; Kane, C. L. *Rev. Mod. Phys.* **2010**, *82*, 3045–3067.
- (12) Moore, J. E. *Nature* **2010**, *464*, 194–198.
- (13) Qi, X. L.; Zhang, S. C. *Rev. Mod. Phys.* **2011**, *83*, 1057–1110.
- (14) Hsieh, T. H.; Lin, H.; Liu, J. W.; Duan, W. H.; Bansil, A.; Fu, L. *Nat. Commun.* **2012**, *3*, 982.
- (15) Tanaka, Y.; Ren, Z.; Sato, T.; Nakayama, K.; Souma, S.; Takahashi, T.; Segawa, K.; Ando, Y. *Nat. Phys.* **2012**, *8*, 800–803.
- (16) Xu, S. Y.; Liu, C.; Alidoust, N.; Neupane, M.; Qian, D.; Belopolski, I.; Denlinger, J. D.; Wang, Y. J.; Lin, H.; Wray, L. A.; Landolt, G.; Slomski, B.; Dil, J. H.; Marcinkova, A.; Morosan, E.; Gibson, Q.; Sankar, R.; Chou, F. C.; Cava, R. J.; Bansil, A.; Hasan, M. Z. *Nat. Commun.* **2012**, *3*, 1192.
- (17) Yan, C. H.; Liu, J. W.; Zang, Y. Y.; Wang, J. F.; Wang, Z. Y.; Wang, P.; Zhang, Z. D.; Wang, L. L.; Ma, X. C.; Ji, S. H.; He, K.; Fu, L.; Duan, W. H.; Xue, Q. K.; Chen, X. *Phys. Rev. Lett.* **2014**, *112*, 186801.
- (18) Liu, J. W.; Hsieh, T. H.; Wei, P.; Duan, W. H.; Moodera, J.; Fu, L. *Nat. Mater.* **2014**, *13*, 178–183.
- (19) Heiss, W.; Groiss, H.; Kaufmann, E.; Hesser, G.; Böberl, M.; Springholz, G.; Schäffler, F.; Koike, K.; Harada, H.; Yano, M. *Appl. Phys. Lett.* **2006**, *88*, 192109.
- (20) Jin, S. Q.; Wu, H. Z.; Xu, T. N. *Appl. Phys. Lett.* **2009**, *95*, 132105.
- (21) Cai, C. F.; Jin, S. Q.; Wu, H. Z.; Zhang, B. P.; Hu, L.; McCann, P. J. *Appl. Phys. Lett.* **2012**, *100*, 182104.
- (22) Kikkawa, J. M.; Smorchkova, I. P.; Samarth, N.; Awschalom, D. D. *Science* **1997**, *277*, 1284–1287.
- (23) Stoger, G.; Brunthaler, G.; Bauer, G.; Ismail, K.; Meyerson, B. S.; Lultz, J.; Kuchar, F. *Semicond. Sci. Technol.* **1994**, *9*, 765–771.
- (24) Morkoc, H.; Cingolani, R.; Gil, B. *Solid-State Electron.* **1999**, *43*, 1909–1927.
- (25) Li, J. H.; Moss, S. C.; Zhang, Y.; Mascarenhas, A.; Pfeiffer, L. N.; West, K. W.; Ge, W. K.; Bai, J. *Phys. Rev. Lett.* **2003**, *91*, 106103.
- (26) Heiss, W.; Groiss, H.; Kaufmann, E.; Hesser, G.; Böberl, M.; Springholz, G.; Schäffler, F.; Koike, K.; Harada, H.; Yano, M. *Appl. Phys. Lett.* **2006**, *88*, 192109.

- (27) Shabani, J.; McFadden, A. P.; Shojaei, B.; Palmstrøm, C. J. *arXiv:1408.2318*, preprint **2014**.
- (28) Analytis, J. G.; McDonald, R. D.; Riggs, S. C.; Chu, J. H.; Boebinger, G. S.; Fisher, I. R. *Nat. Phys.* **2010**, *6*, 960–964.
- (29) Svane, A.; Christensen, N. E.; Cardona, M.; Chantis, A. N.; Schilfgaarde, M. V.; Kotani, T. *Phys. Rev. B* **2010**, *81*, 245120.
- (30) Murakawa, H.; Bahramy, M. S.; Tokunaga, M.; Kohama, Y.; Bell, C.; Kaneko, Y.; Nagaosa, N.; Hwang, H. Y.; Tokura, Y. *Science* **2013**, *342*, 1490–1493.
- (31) Zhang, Y. B.; Tan, Y. W.; Stormer, H. L.; Kim, P. *Nature* **2005**, *438*, 201–204.
- (32) Miao, M. S.; Yan, Q.; Van der Walle, C. G.; Lou, W. K.; Li, L. L.; Chang, K. *Phys. Rev. Lett.* **2012**, *109*, 186803.
- (33) Xiong, J.; Khoo, Y.; Jia, S.; Cava, R. J.; Ong, N. P. *Phys. Rev. B* **2013**, *88*, 035128.
- (34) Zhang, B. P.; Cai, C. F.; Hu, L. A.; Wei, X. D.; Wu, H. Z. *Appl. Surf. Sci.* **2011**, *257*, 1986–1989.